A closed-loop neurobotic system for fine touch sensing

L L Bologna[1,5]**, J Pinoteau**[1,5]**, J-B Passot**[1]**, J A Garrido**[2]**, J Vogel**[3]**, E Ros Vidal**[4]** and A Arleo**[1,6]

[1] Adaptive Neuro Computation Group, Unit of Neurobiology of Adaptive Processes, UMR 7102, CNRS—University Pierre and Marie Curie P6, F-75005 Paris, France
[2] Department of Brain and Behavioral Sciences, University of Pavia, I-27100 Pavia, Italy
[3] Institute of Robotics and Mechatronics, German Aerospace Center (DLR), D-82230 Wessling, Germany
[4] Departamento de Arquitectura y Tecnología de Computardores, University of Granada, E-18071, Granada, Spain

E-mail: angelo.arleo@upmc.fr

Abstract

Objective. Fine touch sensing relies on peripheral-to-central neurotransmission of somesthetic percepts, as well as on active motion policies shaping tactile exploration. This paper presents a novel neuroengineering framework for robotic applications based on the multistage processing of fine tactile information in the closed action–perception loop. *Approach.* The integrated system modules focus on (i) neural coding principles of spatiotemporal spiking patterns at the periphery of the somatosensory pathway, (ii) probabilistic decoding mechanisms mediating cortical-like tactile recognition and (iii) decision-making and low-level motor adaptation underlying active touch sensing. We probed the resulting neural architecture through a Braille reading task. *Main results.* Our results on the peripheral encoding of primary contact features are consistent with experimental data on human slow-adapting type I mechanoreceptors. They also suggest second-order processing by cuneate neurons may resolve perceptual ambiguities, contributing to a fast and highly performing online discrimination of Braille inputs by a downstream probabilistic decoder. The implemented multilevel adaptive control provides robustness to motion inaccuracy, while making the number of finger accelerations covariate with Braille character complexity. The resulting modulation of fingertip kinematics is coherent with that observed in human Braille readers. *Significance.* This work provides a basis for the design and implementation of modular neuromimetic systems for fine touch discrimination in robotics.

S Online supplementary data available from stacks.iop.org/JNE/10/046019/mmedia

(Some figures may appear in colour only in the online journal)

---

1. Introduction

Active tactile perception relies on multistage information processing and adaptive sensorimotor control (Johansson and Flanagan 2009). During haptic recognition tasks, fine touch discrimination is peripherally mediated by fingertip mechanoreceptor responses, which then propagate along the ascending somatosensory pathway towards central areas. Mechanoreceptors densely innervate the dermis of the

fingertips and encode mechanical skin indentations into spike patterns. Single-unit recordings of primary afferents in humans and primates have demonstrated the efficacy (in terms of reliable and fast neurotransmission) of the mechanoreceptors' spatiotemporal code (Johansson and Birznieks 2004, Saal *et al* 2009, Brasselet *et al* 2011b, Mackevicius *et al* 2012). Peripheral nerve fibres transmit mechanoreceptor responses to second-order neurons in the cuneate nucleus of the brainstem according to a somatotopic organization (Whitsel *et al* 1969, Fyffe *et al* 1986b, Leiras *et al* 2010). Cuneate neurons decode and re-encode primary signals prior to their transmission to thalamic and subsequently to cortical areas that mediate downstream experience-dependent haptic percepts (Fyffe *et al* 1986a, Marino *et al* 2001). Ultimately, adaptive control closes the perception–action loop subserving active haptic sensing, e.g. for object manipulation and recognition (Johansson and Flanagan 2009). For this, motor control processes and sensory systems tightly interact to optimize information acquisition. Sensory signals are used to modulate movement policies and generate exploratory behaviours, notably through the anticipation of future sensory inputs (Lederman and Klatzky 1993, Grant *et al* 2009). Conversely, motor signals are used through mechanisms such as efference copy (Blakemore *et al* 2000) or more broadly corollary discharge (Crapse and Sommer 2008) to compensate for misleading re-afferent information, i.e. sensory signals resulting from the movement choice.

An extensive body of experimental and theoretical research has characterized the responses of cutaneous mechanoreceptors to a variety of tactile stimuli (Phillips *et al* 1990, Johansson and Birznieks 2004, Saal *et al* 2009, Brasselet *et al* 2011b, Mackevicius *et al* 2012). In addition, some works have modelled primary afferent activity in monkeys (Freeman and Johnson 1982, Bensmaïa 2002, Kim *et al* 2010) and humans (Bologna *et al* 2011), and a few neurocomputational studies have focused on second-order processing at the cuneate level (Sánchez *et al* 2006, Brasselet *et al* 2009).

However, to the best of our knowledge, a unified framework mirroring the multistage neural coding underlying peripheral-to-central transmission of fine tactile percepts and their use for active exploration remains to be proposed. In an attempt to address this need, we set forth a closed-loop neurobotic system to perform fine touch discrimination through active sensing policies. The proposed architecture accounts for feed-forward neural encoding/decoding processes occurring at the first- and second-order somatosensory stages (i.e. mechanoreceptors and cuneate neurons, respectively). It then emulates a downstream Bayesian probabilistic decoder allowing fine tactile percepts to be discriminated. Finally, both a high-level controller and a low-level cerebellar-like network drive motor adaptation to shape fingertip kinematics.

In this work we employed a Braille reading protocol as a benchmark task. While scanning a Braille dotted line, fine texture perception, decision-making, and adaptive motor control processes cooperate to optimize tactile recognition (Mousty and Bertelson 1985, Bertelson *et al* 1985, Millar 1997, Breidegard *et al* 2006, Breidegard 2007). Recent experimental findings have shown that a Braille reader's fingertip undergoes a previously unreported number of accelerations during character scanning (Hughes *et al* 2011). These changes in velocity are preserved across subjects and appear to depend on both unconscious low-level motor control mechanisms and cognitive (i.e. linguistic) processes (Mousty and Bertelson 1992, Hughes *et al* 2011, Hughes 2011).

The design and implementation of neuromimetic architectures based on neural coding principles and active sensing for fine tactile perception have a two-fold objective. On the neural engineering side, accounting for optimality principles behind neural tactile coding may help in embedding neuroprosthetic devices (Nicolelis and Lebedev 2009, Hochberg *et al* 2012) with biologically plausible sensory feedbacks conveyed peripherally (Raspopovic *et al* 2012) rather than centrally (O'Doherty *et al* 2011). Also, the implementation of neuromorphic sensing technologies (based on spike codes) may foster the development of haptic robotics for real-world applications (Dahiya *et al* 2010). Indeed, although numerous examples of active sensing in closed-loop robotics exist, they primarily focus on coarse tactile perception and grasping-related aspects (Howe 1993, Asfour *et al* 2008, Saal *et al* 2010, Chitta *et al* 2011, Romano *et al* 2011, Bekiroglu *et al* 2011, Yousef *et al* 2011, Petrovskaya and Khatib 2011), whereas relatively few of them address fine touch discrimination (Oddo *et al* 2011, Fishel and Loeb 2012, Su *et al* 2012, Spigler *et al* 2012, Shimojo and Ishikawa 1993). On the neurobiology side, in the mid-term the proposed neuroengineering approach might be useful for testing hypotheses on how primary contact features are encoded/decoded along the ascending somatosensory pathway and used for further processing (Diamond and Arabzadeh 2012, Pleger and Villringer 2013). This approach might then complement neurophysiological investigations through the generation of experimentally testable predictions, e.g. on the optimization of tactile information transfer by second-order cuneate neurons (Bengtsson *et al* 2013).

2. Methods

2.1. System overview

Figure 1(A) shows the complete closed-loop architecture, which included (i) an artificial touch sensor providing an array of analogue responses to mechanical tactile indentations; (ii) a network of primary neurons responsible for transducing the analogue output of the touch sensor into spiking, mechanoreceptor-like, activity; (iii) a network of second-order neurons that, similarly to cuneate neurons of the brainstem, processed primary afferent signals to facilitate downstream tactile discrimination and sensorimotor control; (iv) a probabilistic classification system for tactile input recognition; (v) a high-level controller that shaped active sensing based on optimality classification principles; (vi) a low-level controller subserving cerebellar-like fine movement adaptation; and (vii) a robotic arm-hand setup. Implementation-wise, all these components communicated through user datagram protocol (UDP) channels and were integrated in a framework whose system-clock timestep was 4 ms.
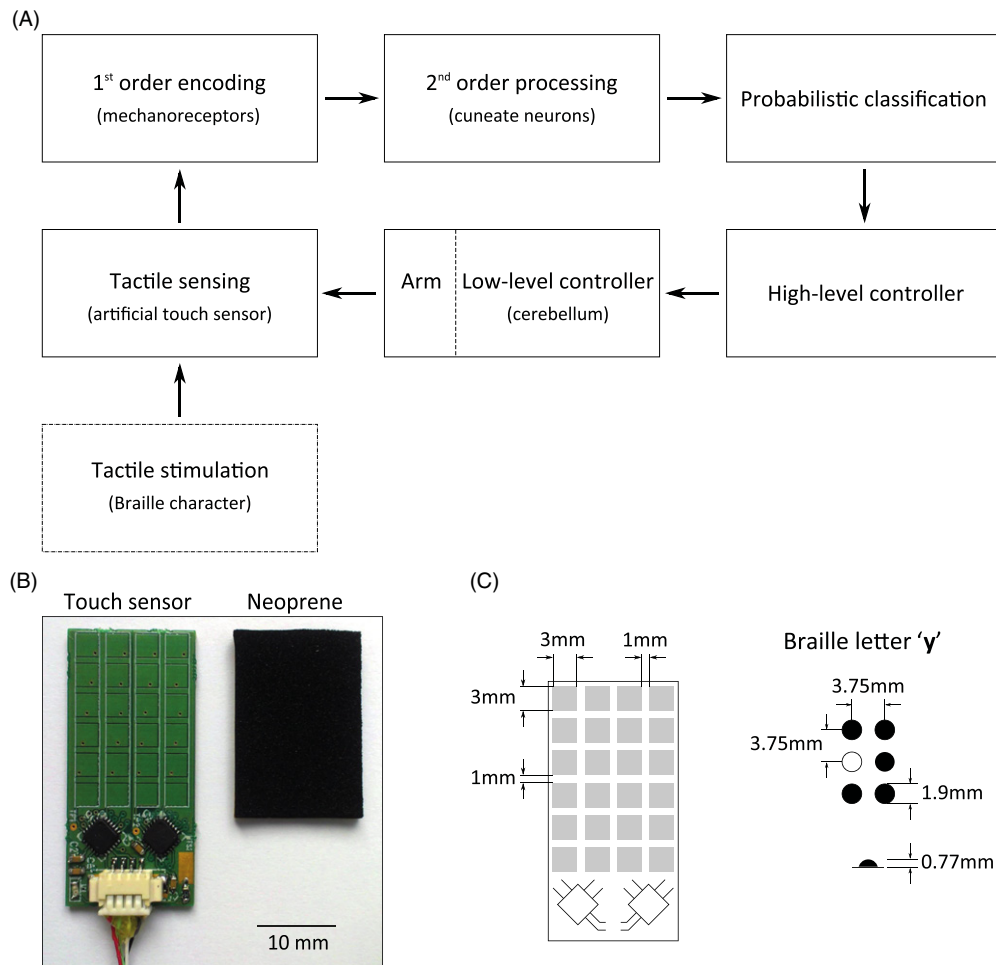
Figure 1. Overview of the closed-loop system and the artificial touch sensor. (A) Clockwise, starting at the bottom left: Braille character-like tactile stimuli indented the artificial touch sensor. A network of first-order neurons mapped the analogue readouts of the touch sensor onto spiking (mechanoreceptor-like) spatiotemporal patterns. Then, a downstream network of second-order neurons processed those primary afferent signals (emulating brainstem cuneate neurons' function) prior to their transmission to a probabilistic classifier. The estimated posterior probability distribution across Braille characters allowed a high-level controller to optimize the active sensing process (by modulating the scanning speed of the fingertip). Finally, a cerebellar-like neural controller provided adaptive low-level adjustments of motor commands before their actual execution by the arm-hand platform. (B) The artificial fingertip consisted of 24 capacitive sensors distributed according to a 6×4 array configuration. A neoprene patch positioned over the touch sensor modulated mechanical indentations. (C) Size-wise comparison between the artificial fingertip (with individual sensor dimensions and inter-sensor distances) and the scaled (1 : 1.7) Braille characters employed for the stimulation protocols.

The tactile stimulation protocol involved a set of 26 different probes reproducing a scaled version (1 : 1.7) of Braille characters (see figure S1 of the supplementary material (available from stacks.iop.org/JNE/10/046019/mmedia)). The artificial fingertip scanned a series of Braille lines actively, which emulated human fingertip deformations exerted by Braille dots. The feed-forward processing mediated by first- and second-order neural networks aimed at allowing rapid and reliable Braille discrimination to be carried out online, under optimized high-level velocity control strategies. We performed a series of quantitative analyses to assess information coding and neurotransmission at both primary and secondary processing stages, to measure performance in terms of fine touch classification, and to characterize adaptive sensorimotor control.

2.2. The artificial touch sensor

The artificial skin prototype[7] (Cannata *et al* 2008, Bologna *et al* 2010) consisted of 24 capacitive square sensors disposed according to a rectangular grid layout (figure 1(B)). A 2.5 mm thick neoprene layer covered the array to protect the sensors during mechanical indentation and to passively modulate the exerted pressure. Each sensor had a dimension of 3 mm and the inter-sensor distance was 1 mm, for a total sensitive surface of approximately 18×23 mm (figure 1(C)). Given the spatial rescaling applied to the system and Braille characters (see section 2.1 of methods), the density of sensors on the artificial skin reached 17 sensor cm^{-2}. A series of preliminary experiments allowed the response properties of the artificial touch sensor to be characterized in the

_____

[7] Developed at the Italian Institute of Technology (IIT), Genoa, Italy.

presence of both static and dynamic stimulation protocols (see supplementary materials, section S2 for more details (available from stacks.iop.org/JNE/10/046019/mmedia)). The analogue response of each sensor had an intensity proportional to the indentation level, with a high signal-to-noise ratio (50 dB), and a Gaussian-shaped profile with a peak amplitude of 200 ± 3.3 (mean $\pm$ std) femtoFarads (fF) and a width of 2.5 ± 0.044 mm. The acquisition frequency of each capacitive pad was 20 Hz.

The dataset of analogue responses collected through these experiments served as a basis for developing a simulated version of the artificial touch sensor. A family of 24 noisy Gaussian kernels sampled the input space based on the spatial location distribution of the real array. Each kernel modelled the response profile of an individual sensor, with white noise added to the amplitude and width of the response, 2.5 fF and 0.1 mm respectively. Also, a Gaussian noise on the position of each simulated stimulus (std = 0.1 mm) accounted for possible positional errors during real stimulation conditions.

2.3. First-order tactile encoding: analogue-to-spike transduction

The analogue readouts $A_i(t)$, with $i \in [1, 24]$, provided by the artificial touch sensor formed the excitatory inputs to a network of spiking neurons, based on a one-to-one connection scheme (figure 2(A)). This network of first-order neurons acted as a population of cutaneous fingertip mechanoreceptors, which converted analogue skin deformations following mechanical indentations onto spiking spatiotemporal patterns.

We implemented the dynamics of each first-order neuron's membrane potential $V_i(t)$ according to a leaky integrate-and-fire model (Lapicque 1907):

$$C \cdot \frac{dV_i(t)}{dt} = -g \cdot (V_i(t) - V') - k \cdot A_i(t) \tag{1}$$

with $C = 0.5$ nF denoting the membrane capacitance, $g = 25$ nS the passive conductance (which gives a membrane time constant equal to $\tau = C/g = 20$ ms), and $V' = -70$ mV the resting membrane potential. The term $k \cdot A_i(t)$ denotes the depolarizing input current, whose intensity was computed by multiplying the analogue response of the afferent touch sensor $A_i(t)$ by a gain factor of $k = -390$ pA/fF, determined by comparing the output spike trains of simulated first-order neurons against recorded mechanoreceptor responses (Johansson and Birznieks 2004).

Each neuron emitted an action potential (spike) whenever its membrane potential $V_i(t)$ reached a threshold $V_{th}(t)$. Immediately after a spike event, the neuron was hyperpolarized to $V_i(t) = V_{reset} = -100$ mV, and the dynamics of its membrane potential were frozen during a refractory period $\Delta t_{ref} = 2$ ms. We also modelled the spiking adaptation phenomenon by means of a 'threshold fatigue' (Chacron *et al* 2003), which consisted of increasing the threshold V_{th} by 50 mV following each neuron discharge, making it harder for the neuron to spike again (i.e. bounding its response firing

rate). In the absence of spikes, V_{th} decreased exponentially back to its resting value V'_{th}:

$$\frac{dV_{th}(t)}{dt} = -\frac{V_{th}(t) - V'_{th}}{\tau_{th}} \tag{2}$$

with $\tau_{th} = 100$ ms, and $V'_{th} = -50$ mV.

2.4. Second-order processing of tactile primary afferents

Second-order processing along the implemented somatosensory pathway occurred through a downstream network of spiking neurons (figure 2(A)), modelling a population of brainstem cuneate cells. The latter constitute the first relay mediating peripheral-to-central transmission of haptic signals (Johansson and Flanagan 2009). The neural model used in this study is derived from a previous work based on neurophysiological data from cat cuneate neurons (Bengtsson *et al* 2013).
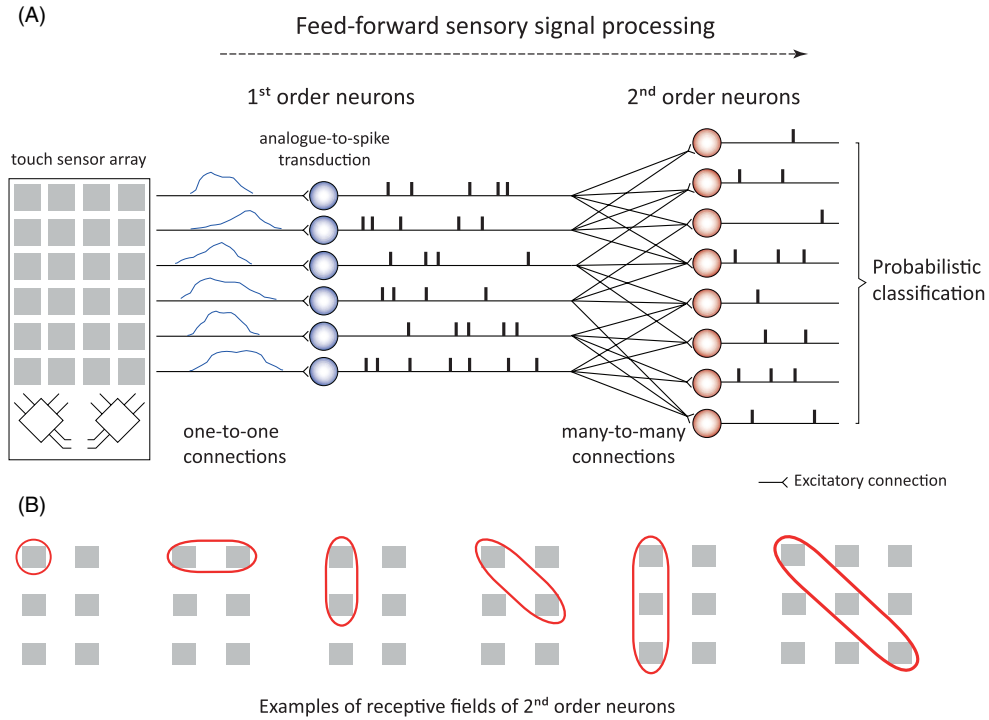
The excitatory projections from first- to second-order neurons followed a scheme so as to generate the receptive fields shown in figure 2(B). Each cuneate neuron received non-plastic afferents from either one or several adjacent mechanoreceptors, with on average 1.9 ± 0.6 (mean $\pm$ std) connections per cuneate neuron. This sparse connectivity is coherent with physiological observations in which only a few primary afferents (less than ten), out of the hundreds of existing connections (Jones 2000), functionally contribute to individual cuneate neuron inputs (Bengtsson *et al* 2013). The dimension and shape of the receptive fields and the synaptic weight distribution of the mechanoreceptor-to-cuneate projections allowed topographical information to be maintained at the level of the second-order output space. The adopted connectivity layout enabled cuneate neurons collecting signals from larger receptive fields to account for both single primary neuron activation and coincidence detection of multiple co-activations, thus enriching their coding dynamics.

We described the activity of each cuneate neuron according to the spike-response model (Gerstner and Kistler 2002), by incorporating a noise model (i.e. escape noise) that followed a stochastic process, thereby providing a linear probabilistic neuronal model (Brasselet *et al* 2009). Whenever multiple afferent spikes excited the neuron within a short time window, they induced a compound membrane potential depolarization equal to:

$$V(t) = V' + \sum_{i,j} w_i \cdot \Delta V(t - \hat{t}_i^j) \tag{3}$$

$$\Delta V(t) \propto \sqrt{t} \cdot \exp(-t/\tau) \tag{4}$$

with $V' = -70$ mV denoting the resting potential, i the presynaptic neurons, and j indexing the spikes emitted by a presynaptic neuron i at times $\hat{t}_i^j$. The synaptic weight w_i of the projection from the presynaptic unit i was taken so as to guarantee a reliable transmission of primary afferent signals and to avoid saturation of second-order neuron activity. We chose $w_i = 0.04$ and $w_i = 0.028$ for mechanoreceptors belonging to cuneate units receptive fields populated by one and two/three units respectively (figure 2(B)). The function $\Delta V(t)$ represented a unitary excitatory postsynaptic potential

(A)

Feed-forward sensory signal processing

1st order neurons

2nd order neurons

touch sensor array

analogue-to-spike transduction

Probabilistic classification

one-to-one connections

many-to-many connections

⊸ Excitatory connection

(B)

Examples of receptive fields of 2nd order neurons

Figure 2. Feed-forward tactile processing mediated by first- and second-order neural populations. (A) The implemented ascending somatosensory pathway. From left to right: the analogue outputs from the artificial touch sensor fed a network of 24 first-order neurons according to a one-to-one projection layout. This early processing stage allowed analogue sensory inputs following mechanical indentation to be converted into spike train patterns, mimicking fingertip mechanoreceptors. Then, a downstream network of 49 spiking neurons decoded and re-encoded primary afferent signals, acting as a sub-population of second-order cuneate neurons in the brainstem. The spatiotemporal output of this second-order network served for a probabilistic classification of fine touch stimuli. (B) The many-to-many connection scheme used to drive second-order neurons gave rise to receptive fields sampling either unitary or multiple primary afferent activity (up to three adjacent mechanoreceptors).

(EPSP), with $\tau = 2$ ms indicating the decay time constant of the EPSP profile.

At each time step, the spiking probability $p(t)$ of the neuron depended on the following functions:

$$p(t) = 1 - \exp(-f(t) \cdot R(t)) \qquad (5)$$

$$f(t) = r_0 \cdot \log\left(1 + \exp\left(\frac{V(t) - V_{\text{th}}}{V_{\text{f}}}\right)\right) \qquad (6)$$

$$R(t) = \frac{(t - \hat{t} - \tau_{\text{abs}})^2}{\tau_{\text{rel}}^2 + (t - \hat{t} - \tau_{\text{abs}})^2} H(t - \hat{t} - \tau_{\text{abs}}) \qquad (7)$$

with $f(t)$ denoting the instantaneous firing rate, determined by the constant $r_0 = 11$ Hz, the threshold potential $V_{\text{th}} = -65$ mV, and a gain factor $V_{\text{f}} = 0.1$ mV. The function $R(t)$ determined the refractoriness property of the neuron, with $\hat{t}$ indicating the time of the last spike emitted, $\tau_{\text{abs}} = 3$ ms the time constant of the absolute refractory period, $\tau_{\text{rel}} = 9$ ms the time constant of relative refractory period, and H the Heaviside function.

We employed the Event-Driven neural simulator based on LookUp Tables (EDLUT)[8] simulation environment (Ros *et al* 2006) to implement the second-order processing stage mediated by the network of model cuneate neurons. EDLUT is designed for efficient simulation of complex neural network models and takes advantage of both time-driven and event-drive procedures so as to guarantee fast computation and

updates of neural state variables (Garrido *et al* 2011). Thanks to its properties, the EDLUT environment provided our system with the computational efficiency required for neurobotic applications.

2.5. Probabilistic classification of tactile percepts

In order to perform *online* tactile discrimination during Braille reading tasks, we trained a naïve Bayesian classifier (NBC) via multinomial distributions (McCallum and Nigam 1998). The NBC belongs to the family of probabilistic classifiers relying on Bayes' rule to compute the posterior probability of sample classes (Duda *et al* 2001). Relying on the hypothesis of independence between features, the NBC provides fast classification and is suited for applications requiring either a frequent estimation of class likelihoods or strict execution-time constraints (e.g. closed-loop systems, real-time robotic applications).

The spatiotemporal patterns provided by second-order cuneate neurons worked as class features, whose posterior probabilities could be incrementally estimated as spikes flew in the NBC—see supplementary materials, section S3 for details (available from stacks.iop.org/JNE/10/046019/mmedia), and Truccolo *et al* (2008) for a previous application of the NBC to recorded neural activity. The NBC training procedure involved a sample base of 100 trials (scans) for each Braille character. A gradually increasing temporal window allowed

---

[8] EDLUT is an open source project freely available at http://edlut.googlecode.com.

the spatiotemporal readouts from the cuneate network to be mapped onto a spike count data vector in a cumulative manner (see figure S3A of the supplementary material (available from stacks.iop.org/JNE/10/046019/mmedia)). Using these data vectors, the NBC computed the posterior probability of a letter being read to correspond to a known character class every 4 ms timestep. For online classification, we averaged the resultant probability distribution (across all Braille characters) over a 40 ms history, and as soon as the mean peak of the probability distribution exceeded the 90% threshold we considered the NBC to have classified the currently scanned Braille character.

2.6. High-level speed controller

The shape of the posterior probability distribution estimated by the NBC across all Braille letters evolved over time as the artificial fingertip scanned a given character. The ongoing degree of peakedness of this probability distribution provided a simple and effective basis to optimize the scanning speed control. A decision-making module (algorithmically implemented) monitored the evolution of the excess Kurtosis index $k(t)$ of the NBC's output probability distribution on a 4 ms timestep basis. The fingertip scanning speed $v(t)$ was then modulated according to:

$$\dot{v}(t) = \frac{k(t) - k(t-1)}{C \cdot v(t)} \tag{8}$$

with $\dot{v}(t)$ denoting the scanning acceleration (cm s^{-2}), and C a constant factor tuned to 600 cm^2 s^{-2}. An increase of the $k(t)$ function indicated a narrowing of the distribution, reflecting a decrease in the uncertainty of the probabilistic classification of the character being scanned. The high-level controller consequently increased the scanning speed proportionally to the gradient value. By contrast, a decrease of $k(t)$ indicated a broadening of the estimate distribution, which induced a deceleration of the fingertip.

2.7. Adaptive low-level controller and robotic arm

In order to compensate for movement execution errors, the closed-loop architecture incorporated a low-level controller (figure 1(A)) responsible for online sensorimotor adaptation. The low-level controller consisted of a spiking neural network mimicking the role of the cerebellum in fine movement control and coordination (Ito 1974, Thach *et al* 1992, Miall *et al* 2001, Attwell *et al* 2002).

We modelled the main information processing stages of the cerebellar microcomplex (see figure S4 of the supplementary material (available from stacks.iop.org/JNE/10/046019/mmedia)), and included long-term plasticity mechanisms to adapt its input–output dynamics through training. In agreement with Marr–Albus–Ito theory (Marr 1969, Albus 1971, Ito and Kano 1982), we assumed that the cerebellum can learn internal representations of sensorimotor interactions in multiple microcomplexes (Wolpert *et al* 1998). We implemented four cerebellar microcomplexes and trained them to predict the outcomes of motor commands prior to their actual execution, i.e. the

microcomplexes acted as forward predictor models (Ito 1984, Miall *et al* 1993, Wolpert and Miall 1996). These predictions allowed the motor commands to be finely adjusted online, by avoiding otherwise inaccurate movement execution (e.g. local drifts in trajectories). See supplementary materials, section S4 (available from stacks.iop.org/JNE/10/046019/mmedia) for a more detailed description of the cerebellar model, which we developed in a previous work (Passot *et al* 2012).

We simulated a 2-dof robotic arm with noisy dynamics, taken from Carrillo *et al* (2008). The arm model included two joints (shoulder, elbow), with the arm end-point carrying the simulated touch sensor described in section 2.2. The four cerebellar forward models learned to predict the future angular position and velocity of each of the two joints. During movement control, the predicted joint states were algorithmically mapped onto the arm end-point position (in Cartesian coordinates). Then, a trajectory generator (Carrillo *et al* 2008) compared the desired and predicted position of the arm end-point and updated the motor commands consequently.

We also tested the performance of the overall Braille reading system in a real-world scenario. Section 3.5 of the results presents a preliminary experiment in which a robotic arm-hand platform, carrying the real artificial touch sensor, scanned and classified a Braille line (figure 8).

2.8. Assessing neurotransmission reliability: metrical information theory

To quantify the information content of first and second-order neural responses we applied the metrical information theory (Brasselet *et al* 2011b). Unlike Shannon mutual information (Shannon 1948), this measure takes into account the metrical properties of the spike train space (Victor and Purpura 1996, Schreiber *et al* 2003, van Rossum 2001), which proved to be suited to decode the responses of human mechanoreceptors obtained via microneurography recordings (Brasselet *et al* 2011b).

The metrical mutual information $I^*(R; S)$, with R and S denoting the response and stimulus space, respectively, is defined as follows:

$$I^*(R; S) = H^*(R) - H^*(R|S)$$
$$= \sum_{s,r} p(r, s) \log_2 \left(\frac{\sum_{r'} p(r'|s)\phi(r, r')}{\sum_{r'} p(r')\phi(r, r')} \right) \tag{9}$$

where

$$H^*(R) = -\sum_r p(r) \log_2 \left(\sum_{r'} p(r')\phi(r, r') \right) \tag{10}$$

$$H^*(R|S) = \sum_s p(s)H(R|s)$$
$$= -\sum_{s,r} p(r, s) \log_2 \left(\sum_{r'} p(r'|s)\phi(r, r') \right) \tag{11}$$

$$\phi(r, r') = H(D_c - D(r, r')) \tag{12}$$

where $H^*(R)$ and $H^*(R|S)$ are the marginal and conditional metrical entropies, respectively; $p(r)$, with $r \in R$, is the response marginal probability; $p(s)$, with $s \in S$, the stimulus

a priori probability; $p(r|s)$ and $p(r, s)$ the conditional and joint probabilities, respectively. The function $\phi(r, r')$ measures the similarity between two responses, and it is defined as the Heaviside function of the Victor–Purpura distance $D(r, r')$ between two spike trains $r,\ r' \in R$ (Victor and Purpura 1996). The term D_c is the cutoff parameter, and is called the critical distance. For $D(r, r') < D_c$, responses $r,\ r'$ are considered as identical (i.e. $\phi(r, r') = 1$), otherwise they are considered as different. If $D_c = 0$ we recover the Shannon entropy from equation (10).

Optimal information transmission occurs when the metrical mutual information $I^*(R; S)$ is maximized and (at the same time) the conditional entropy $H^*(R|S)$ is minimized. Under this optimality condition, perfect input discrimination is reached (Brasselet *et al* 2011b).

2.9. Quantifying Braille character complexity

Several complexity measures have been established in the field of psychophysics to describe visual (Alexander and Carey 1968, Chipman 1977, Yodogawa 1982) and vibro-tactile stimuli (Horner 1991), attempting to link an objective measure to perceived complexity (Aksentijevic and Gibson 2012). To the best of our knowledge, their extension to the study of the Braille alphabet has concentrated solely around the number of dots as a complexity estimator (Nolan and Kederis 1969, Newman *et al* 1984). In order to study the correlation between Braille letter complexity and movement policy (see section 3.3 of the results), we considered a linear combination of two measures, namely the number of dots *Dot* (Nolan and Kederis 1969) and the number of subsymmetries *Sym* (Alexander and Carey 1968):

$$C = \alpha \cdot Dot + (1 - \alpha) \cdot Sym \qquad (13)$$

where

$$Sym = \sum_{x=1}^{X} \sum_{y=1}^{Y} \left(\sum_{i=1}^{X-x} \sum_{j=1}^{Y-y} i \cdot j \cdot NSym_{(x,y)}(i, j) \right) \qquad (14)$$

with $\alpha = 0.94$. The *Sym* function counted the number of symmetries of each rectangular sub-grid of the Braille character matrix and added them in a sum weighted by the area of the sub-grid; with X and Y referring to the size of the first and second cell dimensions respectively (i.e. 2×3 in the case of Braille cells), and $NSym_{(x,y)}(i, j)$ being the number of symmetries observed in the rectangle of size $i \times j$ at position (x, y). The symmetries considered consisted of vertical, horizontal, and central symmetries for all sub-grid dimensions, as well as both diagonal symmetries when $i = j$.

3. Results

3.1. Characterization of first-order responses to dynamic tactile stimulation

We first compared simulated and real human mechanoreceptor responses to moving Braille probes passively sensed by a steady fingertip (Bologna *et al* 2011). To do so, we reproduced in simulation the experimental protocol used by (Phillips *et al* 1990) to characterize primary afferent representations

of dotted spatial patterns. Braille characters were dynamically swiped at 60 mm s^{-1} over the receptive field of a recorded mechanoreceptor while the fingertip was kept still. Once the stimulus exited the receptive field, its position was shifted by 0.2 mm along the radial-to-ulnar axis, and the process repeated. This procedure allowed the so-called spatial event plot (SEP) (Phillips *et al* 1988) to be constructed from the recorded mechanoreceptor spikes (figure 3(A)). Simulated SEPs, which illustrated the spatiotemporal characteristics of a first-order response to a moving Braille stimulus, were qualitatively similar to those of slow adaptive type I (SA-I) human mechanoreceptors. Receptive field sizes of recorded and simulated afferents were also comparable at, respectively, 4.8 ± 1.2 mm^2 (mean $\pm$ std) and 4.7 ± 1.5 mm^2 after correcting for the scale difference. However, due to mechanical constraints, the modelled receptive fields had little overlap and consequently covered the artificial fingertip with a density of 17 units mm^{-2}, one fourth of the 70 units mm^{-2} reached by their biological counterparts (Phillips *et al* 1990). Nonetheless, they showed a topological stimulus-response mapping, an important property for the encoding of fine spatial discontinuities (Johansson and Flanagan 2009).

Figure 3(B) shows an example of discharge pattern recorded from a simulated first-order neuron in response to a single dot stimulus moving at 30 mm s^{-1}. Responses are shown as a raster plot of spike times (top) and the corresponding poststimulus time histogram (PSTH) (centre) during 150 stimulation trials. The analogue output signal from the indented touch sensor serves as depolarizing current to the model neurons (bottom). The spike timing reliability of the firing pattern was high at the onset of the protraction stimulation phase and decreased with time, as observed for human SA-I mechanoreceptors (Johansson and Flanagan 2009) and more generally in central neurons (Mainen and Sejnowski 1995).

We then compared the first-spike jitter distribution of simulated mechanoreceptors against experimental SA-I data (figure 3(C), top). Despite a time lag of about 2 ms, there was no statistical difference between the two distribution shapes (Kolmogorov–Smirnov, $p > 0.076$). Indeed, when accounting for the 2 ms time lag, we did not observe any statistical difference between the two distribution medians (Mann–Whitney U, $p > 0.11$). A comparison between the interspike interval (ISI) distributions of simulated and real mechanoreceptors (figure 3(C), bottom) showed that the ISI variability of model neurons was smaller than in recorded SA-I afferents, although the medians of the two distributions were statistically equivalent (Mann–Whitney U test, $p > 0.16$). The difference in ISI variability may reflect the viscoelastic properties and more complex dynamics of human skin compared to the artificial finger.

3.2. First and second-order processing of dynamic Braille stimuli

We studied neurotransmission reliability at the first- and second-order stages of the simulated somatosensory pathway. The stimulation protocol consisted in scanning
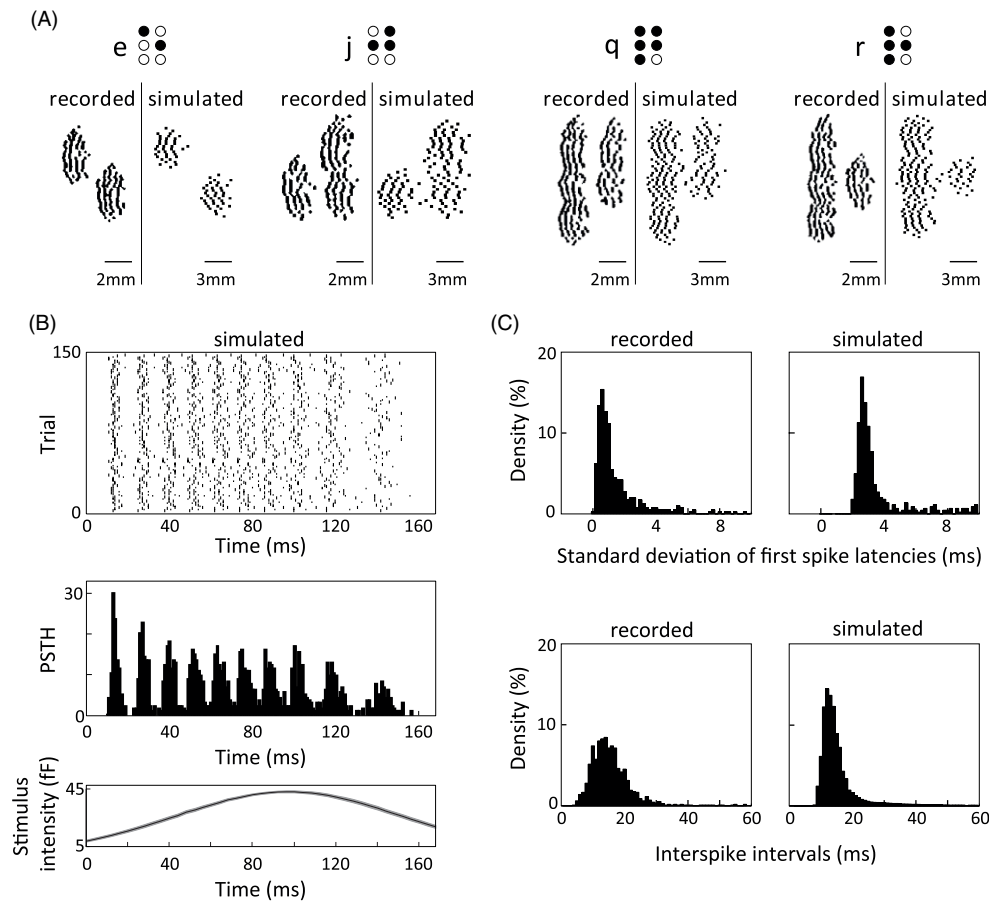
Figure 3. Characterization of first-order responses to dynamic Braille stimulation. (A) Examples of SEPs of human SA-I mechanoreceptor responses to scanned Braille characters (adapted with permission from Phillips *et al* (1990), copyright 1990 Springer), and their simulated counterparts. (B) Spikegram (top) and corresponding PSTH (centre) of 150 responses of a simulated first-order neuron to a single dot stimulus moving at 30 mm s^{-1} (bottom), showing a stronger and better timed activity at the onset of the stimulus. (C) Distributions of standard deviations of first-spike latencies (top) and interspike intervals (bottom) for both real SA-I (left) and simulated (right) mechanoreceptor responses.

the entire 26 character Braille alphabet (see figure S1 of the supplementary material (available from stacks.iop.org/JNE/10/046019/mmedia)) at a constant speed of 30 mm s^{-1} during 200 trials. We performed a metrical information analysis of simulated mechanoreceptor and cuneate responses. Figure 4(A) illustrates the evolution of the information content of first-order and second-order neural activities over time (i.e. as spikes flew in during Braille scanning). At the mechanoreceptor level (figure 4(A), left), a complete discrimination of all Braille characters occurred within 350 ms of stimulus onset, i.e. when the optimality condition was verified. Indeed, according to metrical information theory (Brasselet *et al* 2011b), after 350 ms the clusters of simulated mechanoreceptor responses to all Braille characters became completely separated from each other, allowing perfect context separation to be achieved. Expectedly, the information curve exhibited a plateau after about 100 ms and lasting approximately 75 ms. This time interval corresponded to the stimulation phase during which the fingertip was only contacting the first column of Braille dots, whereas the second column did not yet stimulate any touch sensor. The information value at the plateau was about half of the total information transmitted. We observed a

similar information content profile at the level of simulated cuneate responses (figure 4(A), right), for which perfect input discrimination occurred as rapidly as in first-order neurons. Yet, the redundancy of second-order responses was slightly larger, as indicated by the non-zero conditional metrical entropy after 350 ms.

Even if after 350 ms both mechanoreceptor and cuneate responses contained enough information to discriminate all Braille letters theoretically, we wanted to investigate to what extent the implemented probabilistic decoder would benefit, in terms of classification, from the processing carried out at the cuneate level. We extended the above stimulation protocol by varying the fingertip speed within the range [10, 80] mm s^{-1}, with a step of 10 mm s^{-1}. For each speed value, the fingertip scanned all 26 Braille characters for 100 trials. The performance of the NBC was comparable when decoding first and second-order responses at movement speeds lower than 30 mm s^{-1} (figure 4(B), top). By contrast, processing at the cuneate level led to a statistically significant increase of 12% in classification performance at 30 mm s^{-1} (Mann–Whitney U, $p < 0.01$). The improvement in performance was even larger for higher scanning speeds, showing that cuneate processing enhanced the generalization and robustness of the
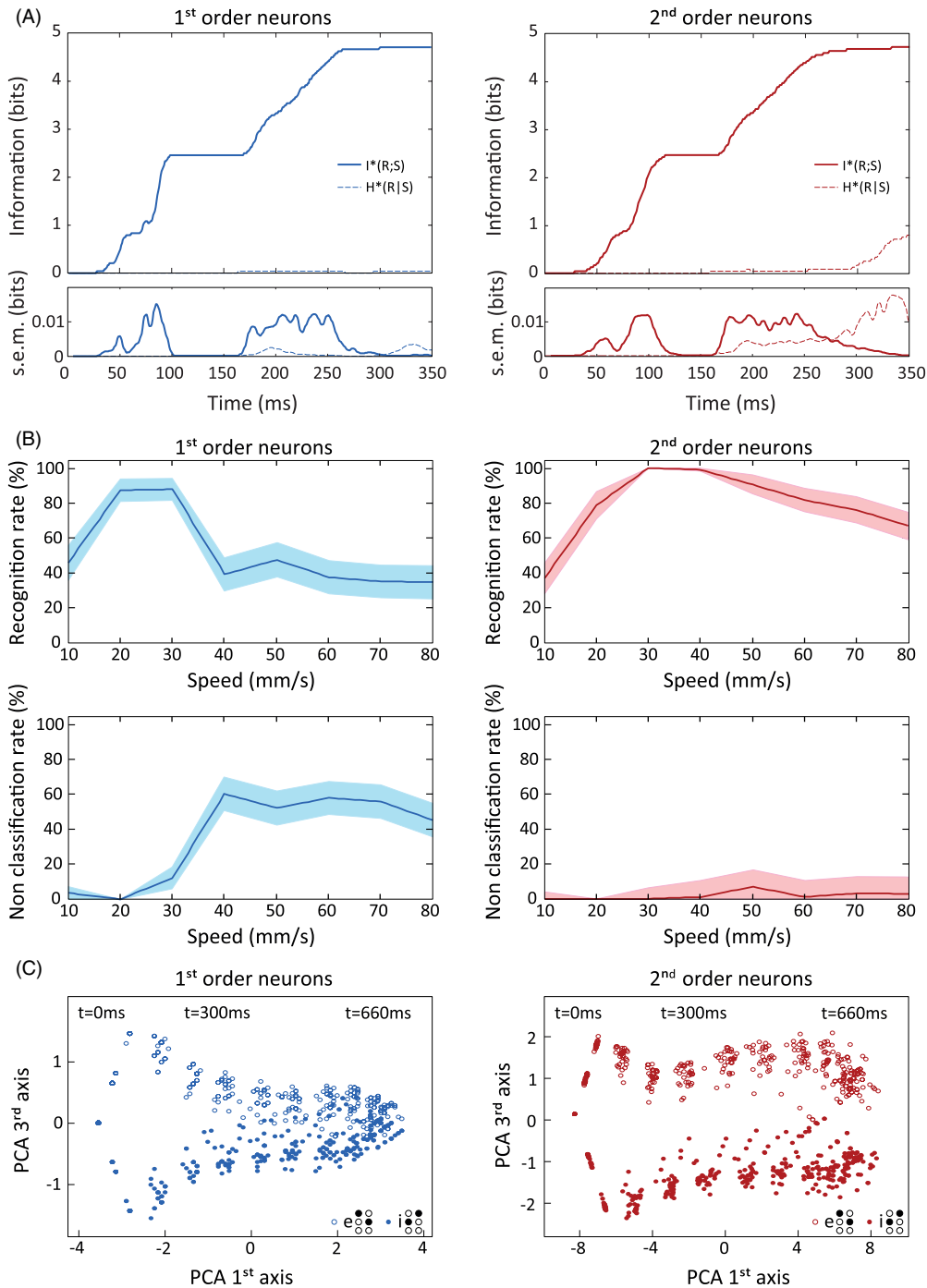
Figure 4. First- and second-order processing of dynamic Braille stimuli. (A) Time course of metrical mutual information (solid curve) and conditional entropy (dashed curve) at the output of first-order neurons (left) and cuneate neurons (right), as the fingertip scans the entire Braille alphabet at 30 mm s^{-1} during 200 trials. The bottom diagrams display the time course of the s.e.m. for both metrical information and condition entropy. (B) Mean recognition rate (top) and nonclassification rate (bottom) when using the NBC to decode first-order activity (left column) and cuneate responses (right column) at different Braille scanning speeds. (C) Principal component analysis on mechanoreceptor (left) and cuneate (right) responses to Braille character 'e' and 'i'. In both cases, the response clusters are projected onto the first and third principal component plane (the second component did not contain any information for distinguishing the two responses).

classification process in the presence of speed modulation. We also quantified the nonclassification rate, i.e. how often, on average, the system was unable to classify a Braille letter during a unique scanning (figure 4(B), bottom). This measure is related to the mean number of reversal movements during Braille reading, which consist of backtracking the fingertip to

rescan a unrecognized letter. In accordance with the above results, for scanning speeds higher than 30 mm s^{-1}, the nonclassification rate was significantly larger when decoding first-order responses than cuneate activity.

To further address this issue, we focused on some Braille dot arrangements that were likely to evoke similar

mechanoreceptor responses due to the homogeneous structure of the artificial touch sensor. For instance, symmetrical letters (e.g. 'e' and 'i', 'd' and 'f', 'h' and 'j' and 'r' and 'w') would activate the same subset of sensors, increasing the probability of cross-character interference during scanning. To illustrate this point we performed a principal component analysis of both first order and cuneate responses obtained at a scanning speed of 30 mm s⁻¹. The example of figure 4(C) shows that the separation between the clusters of first-order responses to letters 'e' and 'i' decreased over time, whereas it remained rather constant at the level of cuneate responses (left and right diagram, respectively). The reduced interference between symmetrical letters at the second-order level partially explains the corresponding better classification performance at higher speeds (figure 4(B)). In the context of the full Braille alphabet, an early discrimination was prevented by interference from letters with identical first dot columns (e.g. 'a', 'c' and 'd' for letter 'e'). In the case of first-order responses, subsequent interference by symmetrical characters left only a small time window available for the classification to occur. For high scanning speeds, this window shortened and the classification performance decreased consequently. By contrast, cuneate processing avoided this effect.

3.3. Online classification of Braille stimuli through closed-loop active sensing

We then tested the performance of the entire closed-loop system, including high- and low-level movement control, in a Braille reading task. The artificial fingertip scanned multiple Braille lines containing 8 letters each, for a total of 200 trials (i.e. repetitions) per letter. As scanning proceeded, feed-forward processing through first and second-order networks provided the probabilistic classifier with continuously evolving spike responses. The NBC estimated the online posterior probability distribution. The latter eventually converged to a narrow single peaked distribution, allowing classification of one Braille letter to be achieved. Figure 5(A) shows the time course of two examples of posterior probability distributions corresponding to the scanning of the letter 'r' (top) and 'e' (bottom). In the first example, early cuneate activity did not allow the probabilistic classifier to distinguish between 'r' and other Braille characters with a similar dot arrangement (i.e. 'l', 'p', 'q', 'v'). Nevertheless, as movement progressed, the probability distribution started to peak, indicating a decrease of uncertainty, until a correct classification became possible.

As shown by the confusion matrix in figure 5(B) and by the distribution in figure 5(C), the overall online classification performance was characterized by a recognition rate of 95±1.5% (mean ± s.e.m), a nonclassification rate (i.e. reversal movement rate) of 1 ± 0.4%, and a false positive rate of 4 ± 1.3%.

Adaptive speed modulation was a function of the evolution of the posterior probability distribution through time, which determined the active sensing policy. The example of figure 6(A) displays the time course of the posterior probability distribution (top) and of the corresponding finger
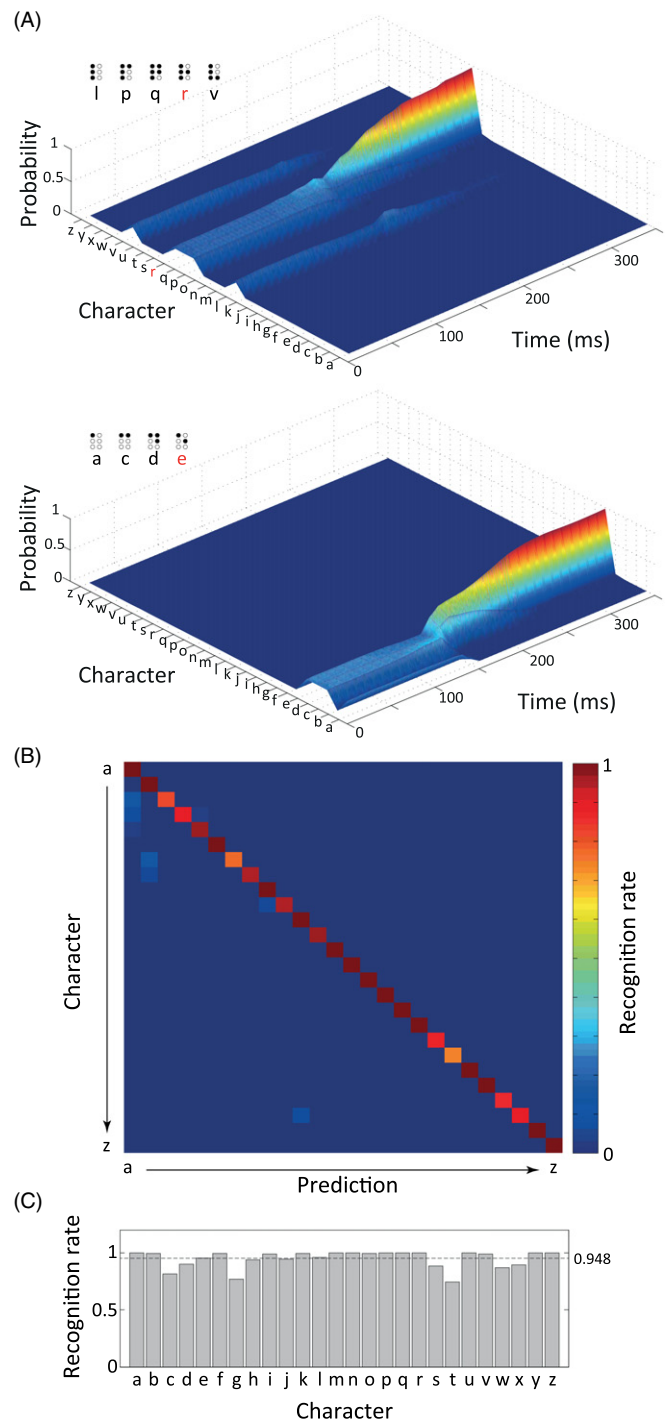
Figure 5. Online classification of Braille stimuli through closed-loop active sensing. (A) Time course of the posterior probability distribution estimated by the NBC when scanning the Braille letter 'r' (top) and 'e' (bottom). (B) Confusion matrix showing the recognition rate and cross-letter interference during online probabilistic classification of Braille characters. The protocol involved 200 scanning trials for each of the 26 letters. (C) Mean recognition rate distribution across the Braille alphabet.

acceleration profile (bottom) while scanning a line with three letters ('d', 'y', and 'n'). Over the entire Braille reading task, the mean number of finger accelerations (both positive and negative) per letter was equal to 11.8, which is of the same order of magnitude as that observed in human
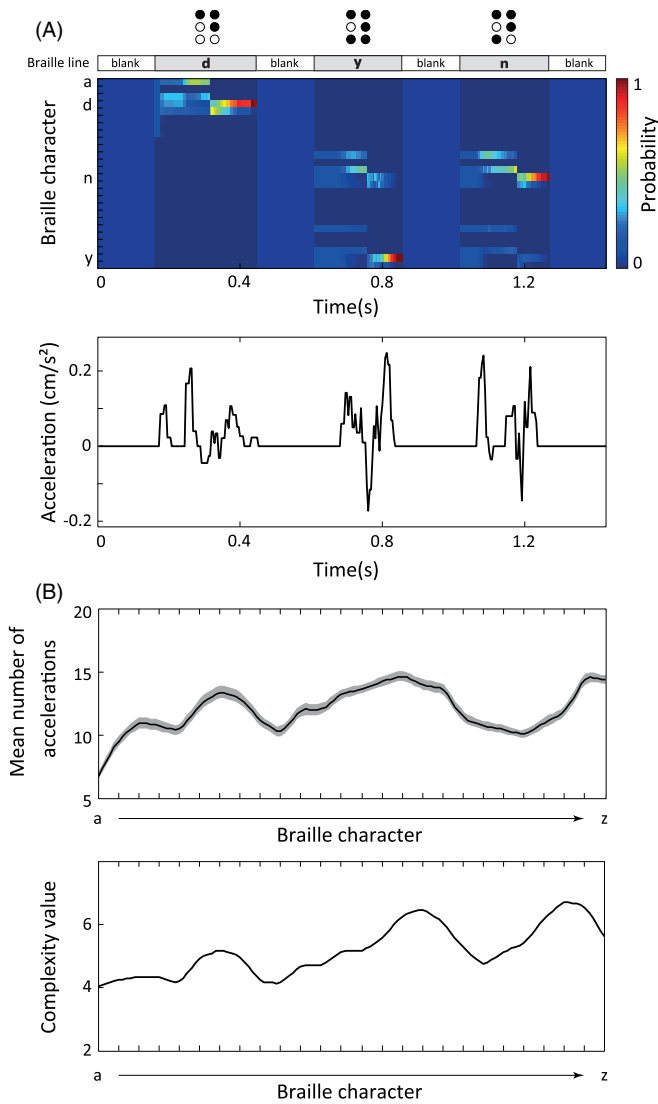
Figure 6. Adaptive modulation of Braille reading speed. (A) Top: example of time course of the posterior probability distribution estimated by the NBC while the fingertip was scanning a Braille line with three letters. Bottom: corresponding online fingertip acceleration profile. (B) Top: mean number of accelerations (both positive and negative) per letter, averaged over 200 repetitions (solid line: mean; grey area: s.e.m.). Accelerations smaller than 0.1 mm s^{-2} were filtered out for this analysis. Bottom: complexity value distribution across all Braille characters.

Braille reading experiments (Hughes 2011, Hughes *et al* 2011). Importantly, the movement policy (and consequently the number of accelerations) varied significantly depending on the letter being scanned (figure 6(B), top; Kruskal–Wallis ANOVA, $p < 0.01$). In addition, we observed a significant correlation between the distribution of Braille character complexity (defined according to equation (13)) and the distribution of the number of accelerations per letter (figure 6(B), bottom; Spearman's $\rho = 0.66$, $p < 10^{-3}$).

3.4. Robustness of fine touch sensing to position errors

During Braille reading, the low-level cerebellar controller adjusted the trajectory of the fingertip online. The training

of the cerebellar network involved ten sessions. Each session consisted of ten trials during which the fingertip (i.e. the end-point of the 2-dof arm carrying the artificial touch sensor) had to scan a Braille line containing eight evenly spaced characters, at a constant command speed of 30 mm s^{-1}. After training, the output of the cerebellar network provided a good estimator of the noisy arm dynamics, allowing motor commands to be tuned online—and, consequently, the movement accuracy to be improved. The mean position error, computed as the discrepancy between desired and actual fingertip trajectory, decreased significantly through cerebellar training, from 0.81 ± 0.04 mm (mean $\pm$ s.e.m) to 0.54 ± 0.04 mm (Mann–Whitney U, $p < 0.01$).

Figure 7(A) shows a sample of fingertip trajectory (top), the corresponding PSTH (centre) of the cerebellar output (i.e. the activity of simulated neurons in the deep cerebellar nuclei (DCN)), and two examples of DCN spikegrams. Figure 7(B) shows a fingertip trajectory, averaged over ten trials, with and without cerebellar-dependent adaptation (blue and red curve, respectively). The cerebellar online adjustment proved effective at reducing fingertip oscillation amplitudes. We quantified the percentage of times that the fingertip trajectory exceeded a ± 1 mm bounded region (dashed lines in figure 7(B)). The resulting error, averaged over 10 trials, decreased significantly through cerebellar training (figure 7(C); Mann–Whitney U, $p < 10^{-3}$). About 82% of the positions belonging to a finger trajectory fell, on average, within the ± 1 mm boundary by the end of training.

We then studied the influence of position inaccuracy on the probabilistic classification performance through the following protocol. A Braille line was swiped at 30 mm s^{-1} over the immobile artificial fingertip. After 80 repetitions of each letter, the Braille line was shifted along the distal-to-proximal axis by 0.5 mm, and the process repeated. This shift corresponded to a fingertip position change along the Y axis in the active sensing scenario. Figure 7(D) shows the recognition rate (mean $\pm$ s.e.m.) as a function of the Y position. The mean classification performance remained high within the ± 1 mm range, whereas it decreased sharply beyond these boundaries. The best recognition rate of 99% occurred at Y positions of 0 and -0.5 mm (Mann–Whitney U, $p > 0.4$). Finally, figure 7(E) displays the classification performance distribution across letters depending on the Y position. The recognition rate of individual letters tended to follow an all-or-none pattern, with few intermediate values.

3.5. Preliminary validation on a real robot performing real-time Braille reading

In order to test the performance of the system in a real-world scenario, we ran a preliminary experiment in which a robotic arm-hand platform had to solve a Braille reading task (figure 8(A)). We fixed the artificial touch sensor (Cannata *et al* 2008) on the index digit of the DLR-HIT hand II (Liu *et al* 2008) (figure 8(B)). Then, we mounted the hand on the DLR light-weight robot III (LWR) (Albu-Schäffer *et al* 2007a), in order to rub the fingertip over a Braille line at a constant speed of 30 mm s^{-1} (figure 8(C)). Both the LWR robot
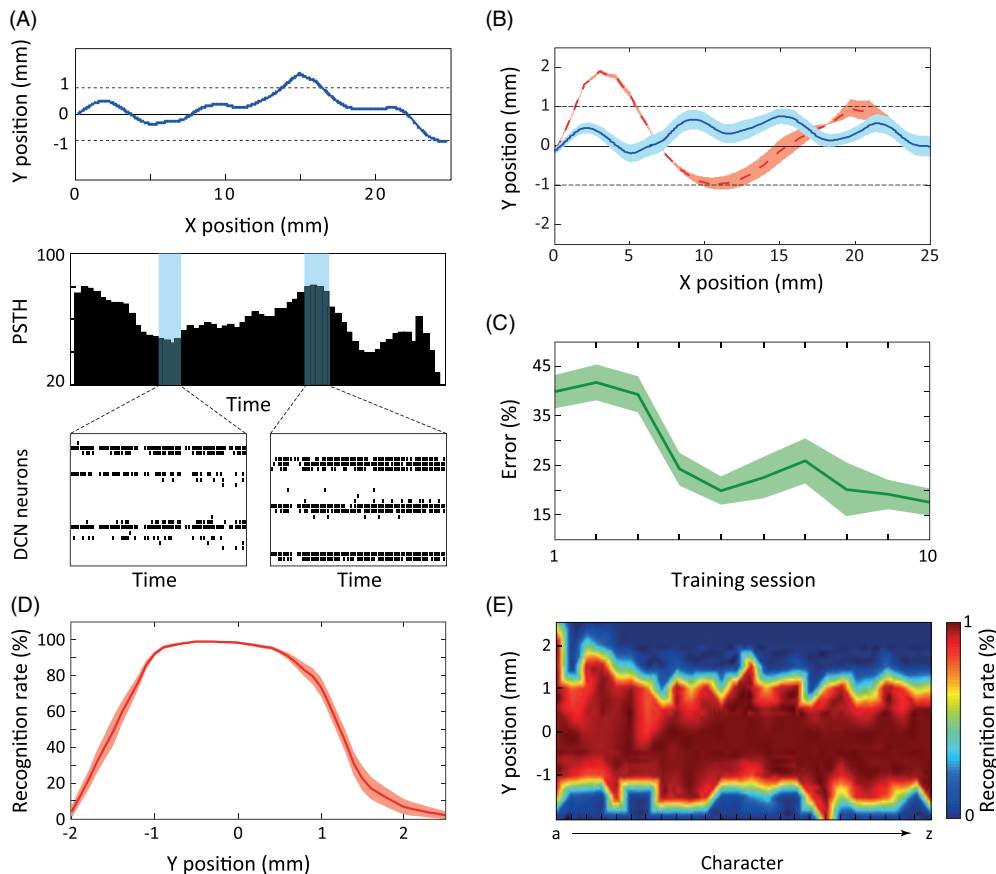
Figure 7. Robustness of fine touch sensing to position errors. (A) Example of fingertip trajectory (top), corresponding PSTH (centre) of the cerebellar output (i.e. activity of simulated deep cerebellar nucleus, DCN, units), and raster plots of DCN spike trains at two different moments of the trajectory (bottom). (B) Fingertip trajectory samples before and after training of the cerebellar low-level controller (dashed red and solid blue curve, respectively). Solid lines indicate mean trajectories averaged over 10 trials, whereas shaded areas delimit the corresponding s.e.m. values. (C) Mean percentage of points of a trajectory exceeding the ±1 mm boundary as a function of cerebellar training sessions. (D) Left: mean recognition rate, averaged over all Braille characters and 80 repetitions per character, as a function of the *Y* position of the finger (the shaded area represents the s.e.m.). Right: distribution of recognition rates across all Braille letters for different *Y* positions.

and the DLR-HIT hand were operated in impedance control mode (Albu-Schäffer *et al* 2007b), which ensured stability even in physical contact situations as required in this task. The calculated adjustments to the reading velocity as well as the corrections to the movement trajectory were relayed to the robotic system via an UDP interface. Yet, compared to the simulated arm, noise in the pitch and roll dynamics of the real arm-hand platform remained marginally compensated, which increased the probability of inhomogeneous and discontinuous contacts between the fingertip and Braille characters.

We selected a subset of representative Braille characters and recorded 150 trials per character. Again, first and second order neural networks mediated feed-forward processing of tactile signals prior to their use for probabilistic classification. We trained the NBC through the same offline procedure used for simulated data, which aimed at estimating the posterior probability distribution through increasing temporal windows that sampled cuneate responses (see supplementary materials, section S3 for details (available from stacks.iop.org/JNE/10/046019/mmedia)). We randomly selected 100 trials for training and we employed the remaining 50 trials for probing Braille character recognition. The mean

classification rate, averaged over seven characters, was 89 ± 5.3% (mean ± s.e.m.; figure 8(D)), with a false positive rate of 11 ± 5.3%. This preliminary robotic validation gave rise to a real-time and online Braille reading demonstrator in the framework of the European project 'Sensopac', no. IST-028056-IP (see supplementary material videos (available from stacks.iop.org/JNE/10/046019/mmedia)).

4. Discussion

This paper presents a closed-loop neural architecture for fine tactile sensing in robotic applications. A Braille reading scenario was chosen as a case study. The system integrated neural coding principles with a probabilistic decision-making framework for input classification and adaptive control.

Tactile processing at the early stages of the somatosensory pathway was emulated by converting the analog readouts from an artificial touch sensor into mechanoreceptor responses (Phillips *et al* 1990). The modelled mechanoreceptors captured some characteristics of real SA-I human primary afferents, in terms of input–output spatial mapping and variability in spike latencies. We quantified the accuracy of primary
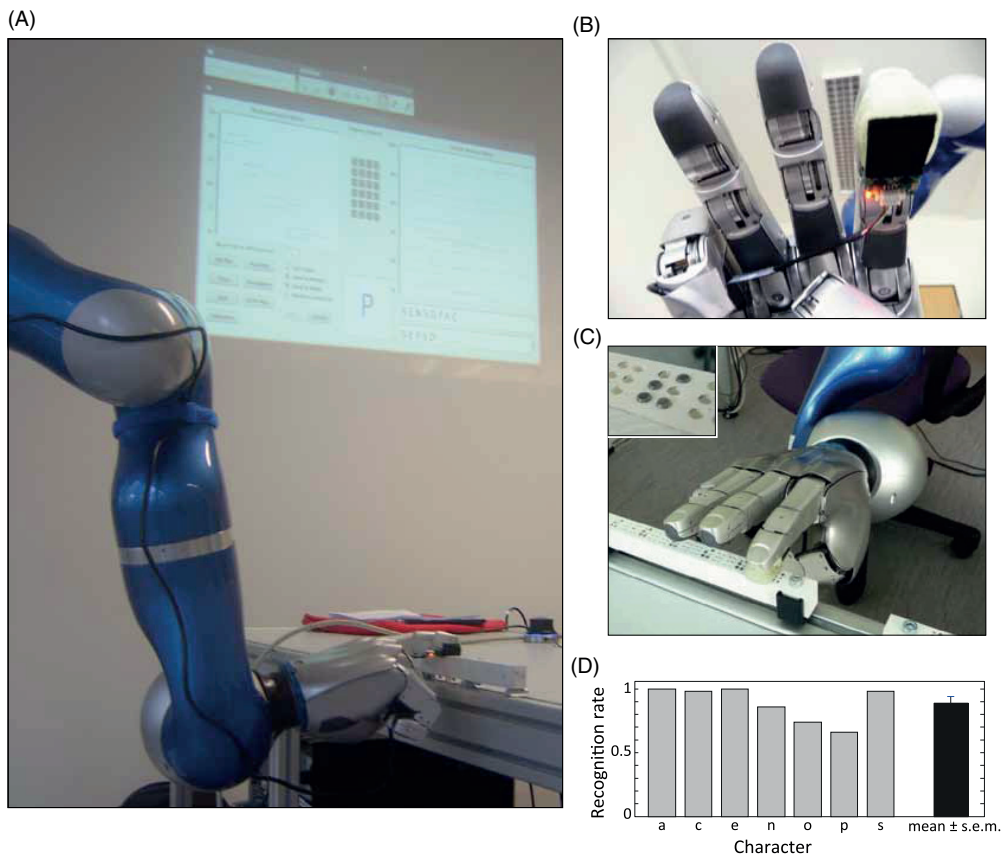
Figure 8. Preliminary validation on a real robotic platform performing real-time Braille reading. (A) The arm-hand robotic platform performing online and real-time Braille reading. The arm was the DLR light-weight robot III (LWR) (Albu-Schäffer *et al* 2007a). (B) The artificial touch sensor (Cannata *et al* 2008) was fixed on the robotic hand DLR-HIT hand II (Liu *et al* 2008). (C) The robotic arm-hand sliding over a Braille line. Inset: a scaled Braille character. (D) Mean recognition rate distribution across a subset of Braille letters, and mean ± s.e.m. values.

contact coding via the same information theoretical tools that we previously used to decode human microneurography recordings (Brasselet *et al* 2011b). The results presented in this paper were consistent with experimental evidence showing that the spatiotemporal structure of mechanoreceptor responses provides highly discriminative touch signals (Johansson and Birznieks 2004). These primary afferent signals were processed by a second-order neural network that, similar to a population of neurons in the cuneate nucleus of the brainstem, mediated peripheral-to-central tactile information transfer (Jones 2000, Hsiao 2008). Our results corroborated the hypothesis that, thanks to a sparse first- to second-order neurons connectivity, cuneate cells might constitute more than a mere synaptic relay along the somatosensory pathway. They may indeed increase input separability to minimize destructive interference and maximize memory capacity in cortical haptic processes.

Downstream from the simulated cuneate layer, a NBC performed Braille character recognition. This probabilistic approach proved to be efficient in discriminating all Braille characters online. NBCs, though inappropriate for regression problems (Frank *et al* 2000), can indeed outperform more sophisticated algorithms when used in categorization tasks, even though the independence assumption is seldom verified in real-world applications. This is mainly due to the fact that

statistical dependences between attributes often cancel each other out or are evenly distributed among classes (Zhang 2004). Also, in categorization tasks a data sample is usually classified according to the highest posterior probability, which often refers to the correct class regardless of its accuracy (Domingos and Pazzani 1996, 1997).

In the designed system, a high- and low-level controller closed the action perception loop by driving active tactile sensing. We studied the pervasive finger accelerations as done for human Braille reading (Hughes *et al* 2011). The origin of fingertip speed changes resides in several mechanisms (e.g. sensorimotor, semantic, linguistic), although it is still unclear which contributions dominate and to what extent (Hughes 2011). For example, sublexical mechanisms were shown to influence the number of accelerations only in specific reading conditions (Hughes 2011). To the best of our knowledge, no extensive study quantitatively explored the relationship between pattern complexity and number of accelerations at the single character resolution. Without seeking for a comprehensive explanation of the origin of finger accelerations, we investigated if a simple probabilistic approach could account for the influence of texture complexity and local ambiguities on finger kinematics. We assumed that the posterior probability distributions estimated during Braille scanning would determine the high-level control of the

finger speed. Our results showed a number of accelerations coherent with experimental observations (Hughes 2011) as well as significantly correlated with the complexity of Braille dot patterns. The implemented low-level controller consisted of a spiking neural network capturing the sensorimotor adaptation function of the cerebellum (Passot *et al* 2012). It allowed finger movements to be finely tuned, thus improving the robustness of the overall closed-loop dynamics during Braille scanning.

The developed neuroengineering framework can be extended to further investigate (i) the neural bases of fine touch processing and active sensing, (ii) neuromorphic-like solutions for humanoid robotics built on the efficiency principles behind neural tactile coding, and (iii) biologically plausible sensory feedbacks for haptic neuroprosthetic applications. At the peripheral level, we are currently investigating the extent to which the known irregular and inhomogeneous properties of mechanoreceptive fields (Phillips *et al* 1992) may be relevant to the encoding of primary contact features. Recent experimental evidence suggests that distinct sub-regions of each receptive field, named hotspots (Phillips *et al* 1992), might increase the spatial resolution of the mechanoreceptors' code (Pruszynski *et al* 2011). We are testing the hypothesis that this increase in encoding resolution may play a role in the extraction of primitive tactile features—e.g. to serve as a basis for the known stimulus orientation selectivity of somatosensory cortical responses (Hsiao *et al* 2002). To this effect, more efficient transduction technologies (Maheshwari and Saraf 2008) will be introduced to replace the current sensors, whose temporal and spatial resolution limit the system's precision. Along the same lines, we are studying the ability of primary afferents to encode stimulus features and create an isomorphic representation of the stimulus space (Brasselet *et al* 2011a). This capability would permit going beyond touch discrimination and input recognition, and it may provide a likely basis for generalization in haptic perception (i.e. the ability to extrapolate tactile recognition from never experienced stimuli). At the second-order level, we are further investigating how unitary and population cuneate activity can optimally process mechanoreceptive signals (Bengtsson *et al* 2013). We are primarily focusing on the possible role of excitatory/inhibitory dynamics in sparsifying cuneate representations of haptic percepts. Secondly, we are studying how spike timing-dependent plasticity (STDP) mechanisms (Bi and Poo 1998) may shape, during development, or reshape, following injury, the connectivity layout of mechanoreceptor-to-cuneate synaptic projections to enhance coding capacity. STDP-like synaptic adaptation, extensively observed in central brain regions, could make cuneate neurons respond selectively to specific spatiotemporal spike patterns and/or extract sub-patterns of activity from complex primary afferent responses (e.g. induced by multi-point stimulation delivered at the fingertip). Finally, taking advantage of the putative sparse code mediated by cuneate neurons, we will implement a spike-based downstream probabilistic classifier. Insights from this ongoing research will further increase the neuromorphic degree of the closed-loop architecture. They will also guide the design of plausible sensory feedback patterns for neuroprosthetic applications, by allowing their efficacy at multiple somatosensory processing stages to be systematically assessed.

Acknowledgments

References

Aksentijevic A and Gibson K 2012 Complexity equals change *Cogn. Syst. Res.* **15** 1–16

Albu-Schäffer A, Haddadin S, Ott C, Stemmer A, Wimbock T and Hirzinger G 2007a The DLR lightweight robot: design and control concepts for robots in human environments *Indust. Robot.* **34** 376–85

Albu-Schäffer A, Ott C and Hirzinger G 2007b A unified passivity-based control framework for position, torque and impedance control of flexible joint robots *Int. J. Robot. Res.* **26** 23–39

Albus J S 1971 A theory of cerebellar function *Math. Biosci.* **10** 25–61

Alexander C and Carey S 1968 Subsymmetries *Percept. Psychophys* **4** 73–77

Asfour T, Azad P, Vahrenkamp N, Regenstein K, Bierbaum A, Welke K, Schroeder J and Dillmann R 2008 Toward humanoid manipulation in human-centred environments *Robot. Auton. Syst.* **56** 54–65

Attwell P J, Cooke S F and Yeo C H 2002 Cerebellar function in consolidation of a motor memory *Neuron* **34** 1011–20

Bekiroglu Y, Laaksonen J, Jorgensen J A, Kyrki V and Kragic D 2011 Assessing grasp stability based on learning and haptic data *IEEE Trans. Robot.* **27** 616–29

Bengtsson F, Brasselet R, Johansson R S, Arleo A and Jörntell H 2013 Integration of sensory quanta in cuneate nucleus neurons *in vivo PloS ONE* **8** e56630

Bensmaïa S J 2002 A transduction model of the Meissner corpuscle *Math. Biosci.* **176** 203–17

Bertelson P, Mousty P and D'Alimonte G 1985 A study of Braille reading: 2. Patterns of hand activity in one-handed and two-handed reading *Q. J. Exp. Psychol.* A **37** 235–56

Bi G Q and Poo M M 1998 Synaptic modifications in cultured hippocampal neurons: dependence on spike timing, synaptic strength, and postsynaptic cell type *J. Neurosci.* **18** 10464–72

Blakemore S-J, Wolpert D and Frith C 2000 Why can't you tickle yourself? *Neuroreport* **11** R11–6

Bologna L L, Brasselet R, Maggiali M and Arleo A 2010 Neuromimetic encoding/decoding of spatiotemporal spiking signals from an artificial touch sensor *Proc. Int. Joint Conf. on Neural Networks* pp 1–6

Bologna L L, Pinoteau J, Brasselet R, Maggiali M and Arleo A 2011 Encoding/decoding of first and second order tactile afferents in a neurorobotic application *J. Physiol.* **105** 25–35

Brasselet R, Johansson R and Arleo A 2009 Optimal context separation of spiking haptic signals by second-order somatosensory neurons *Adv. Neural Inform. Process. Syst.* **22** 180–8

Brasselet R, Johansson R S and Arleo A 2011a Isometric coding of spiking haptic signals by peripheral somatosensory neurons *Advances on Computational Intelligence (Lecture Notes in*

Computer Science vol 6691) ed J E A Cabestany (Berlin: Springer) pp 528–36

Brasselet R, Johansson R S and Arleo A 2011b Quantifying neurotransmission reliability through metrics-based information analysis *Neural Comput.* **23** 852–81

Breidegard B 2007 Computer-based automatic finger- and speech-tracking system *Behav. Res. Methods* **39** 824–34

Breidegard B, Jönsson B, Fellenius K and Strömqvist S 2006 Disclosing the secrets of Braille reading—computer-aided registration and interactive analysis *Vis. Impair Res.* **8** 49–59

Cannata G, Maggiali M, Metta G and Sandini G 2008 An embedded artificial skin for humanoid robots *Proc. IEEE Int. Conf. on Multisensor Fusion and Integration for Intelligent Systems* pp 434–38

Carrillo R R, Ros E, Boucheny C and Coenen O J 2008 A real-time spiking cerebellum model for learning robot control *Biosystems* **94** 18–27

Chacron M J, Pakdaman K and Longtin A 2003 Interspike interval correlations, memory, adaptation, and refractoriness in a leaky integrate-and-fire model with threshold fatigue *Neural Comput.* **15** 253–78

Chipman S F 1977 Complexity and structure in visual patterns *J. Exp. Psychol. Gen.* **106** 269–301

Chitta S, Sturm J, Piccoli M and Burgard W 2011 Tactile sensing for mobile manipulation *IEEE Trans. Robot.* **27** 558–68

Crapse T B and Sommer M A 2008 Corollary discharge across the animal kingdom *Nature Rev. Neurosci.* **9** 587–600

Dahiya R S, Metta G, Valle M and Sandini G 2010 Tactile sensing—from humans to humanoids *IEEE Trans. Robot.* **26** 1–20

Diamond M E and Arabzadeh E 2012 Whisker sensory system—from receptor to decision *Prog. Neurobiol.* **103** 28–40

Domingos P and Pazzani M 1996 Beyond independence: conditions for the optimality of the simple Bayesian classifier *Proc. 13th Int. Conf. on Machine Learning* pp 105–12

Domingos P and Pazzani M 1997 On the optimality of the simple Bayesian classifier under zero-one loss *Mach. Learn.* **29** 103–30

Duda R O, Hart P E and Stork D G 2001 *Pattern Classification* (New York: Wiley-Interscience)

Fishel J A and Loeb G E 2012 Bayesian exploration for intelligent identification of textures *Front. Neurorobot.* **6** 4

Frank E, Trigg L, Holmes G and Witten I H 2000 Technical note: naive Bayes for regression *Mach. Learn.* **41** 5–26

Freeman A W and Johnson K O 1982 Cutaneous mechanoreceptors in macaque monkey: temporal discharge patterns evoked by vibration, and a receptor model *J. Physiol.* **323** 21–41

Fyffe R E, Cheema S S, Light A R and Rustioni A 1986a Intracellular staining study of the feline cuneate nucleus: II. Thalamic projection neurons *J. Neurophysiol.* **56** 1284–96

Fyffe R E, Cheema S S and Rustioni A 1986b Intracellular staining study of the feline cuneate nucleus: I. Terminal patterns of primary afferent fibers *J. Neurophysiol.* **56** 1268–83

Garrido J A, Carrillo R R, Luque N R and Ros E 2011 Event and time driven hybrid simulation of spiking neural networks *Advances in Computational Intelligence (Lecture Notes in Computer Science* vol 6691) ed J Cabestany, I Rojas and G Joya (Berlin: Springer) pp 554–61

Gerstner W and Kistler W M 2002 *Spiking Neuron Models: Single Neurons, Populations, Plasticity* (Cambridge: Cambridge University Press)

Grant R A, Mitchinson B, Fox C W and Prescott T J 2009 Active touch sensing in the rat: anticipatory and regulatory control of whisker movements during surface exploration *J. Neurophysiol.* **101** 862–74

Hochberg L R *et al* 2012 Reach and grasp by people with tetraplegia using a neurally controlled robotic arm *Nature* **485** 372–5

Horner D T 1991 The effects of complexity on the perception of vibrotactile patterns *Percept. Psychophys* **49** 551–62

Howe R D 1993 Tactile sensing and control of robotic manipulation *Adv. Robot.* **8** 245–61

Hsiao S 2008 Central mechanisms of tactile shape perception *Curr. Opin. Neurobiol.* **18** 418–24

Hsiao S S, Lane J and Fitzgerald P 2002 Representation of orientation in the somatosensory system *Behav. Brain. Res.* **135** 93–103

Hughes B 2011 Movement kinematics of the braille-reading finger *J. Vis. Impair Blind* **105** 370–81

Hughes B, Van Gemmert A W A and Stelmach G E 2011 Linguistic and perceptual-motor contributions to the kinematic properties of the braille reading finger *Hum. Mov. Sci.* **30** 711–30

Ito M 1974 *Control Mechanisms of Cerebellar Motor System* (Cambridge, MA: MIT Press) pp 293–303

Ito M 1984 *The Cerebellum and Neural Control* (New York: Raven Press)

Ito M and Kano M 1982 Long-lasting depression of parallel fiber-purkinje cell transmission induced by conjunctive stimulation of parallel fibers and climbing fibers in the cerebellar cortex *Neurosci. Lett.* **33** 253–8

Johansson R S and Birznieks I 2004 First spikes in ensembles of human tactile afferents code complex spatial fingertip events *Nature Neurosci.* **7** 170–7

Johansson R S and Flanagan J R 2009 Coding and use of tactile signals from the fingertips in object manipulation tasks *Nature Rev. Neurosci.* **10** 345–59

Jones E G 2000 Cortical and subcortical contributions to activity-dependent plasticity in primate somatosensory cortex *Annu. Rev. Neurosci.* **23** 1–37

Kim S S, Sripati A P and Bensmaia S J 2010 Predicting the timing of spikes evoked by tactile stimulation of the hand *J. Neurophysiol.* **104** 1484–96

Lapicque L 1907 Recherches quantitatives sur l'excitation électrique des nerfs traitée comme une polarisation *J. Physiol. Pathol. Gén.* **9** 620–35

Lederman S J and Klatzky R L 1993 Extracting object properties through haptic exploration *Acta Psychol.* **84** 29–40

Leiras R, Velo P, Martin-Cora F and Canedo A 2010 Processing afferent proprioceptive information at the main cuneate nucleus of anesthetized cats *J. Neurosci.* **30** 15383–99

Liu H, Wu K, Meusel P, Seitz N, Hirzinger G, Jin MH, Liu Y W, Fan S W, Lan T and Chen Z P 2008 Multisensory five-finger dexterous hand: the DLR/HIT hand II *Proc. IEEE/RSJ Int. Conf. on Intelligent Robots and Systems* pp 3692–97

Mackevicius E L, Best M D, Saal H P and Bensmaia S J 2012 Millisecond precision spike timing shapes tactile perception *J. Neurosci.* **32** 15309–17

Maheshwari V and Saraf R 2008 Tactile devices to sense touch on a par with a human finger *Angew. Chem. Int. Edn. Engl.* **47** 7808–26

Mainen Z F and Sejnowski T J 1995 Reliability of spike timing in neocortical neurons *Science* **268** 1503–6

Marino J, Aguilar J, Soto C and Canedo A 2001 The cerebral cortex modulates the cutaneous transmission through the dorsal column nuclei *Rev. Neurol.* **33** 448–54

Marr D 1969 A theory of cerebellar cortex *J. Physiol.* **202** 437–70

McCallum A and Nigam K 1998 A comparison of event models for naive Bayes text classification *Proc. AAAI-98 Workshop on Learning for Text Categorization* (Menlo Park, CA: AAAI Press) pp 41–48

Miall R C, Reckess G Z and Imamizu H 2001 The cerebellum coordinates eye and hand tracking movements *Nature Neurosci.* **4** 638–44

Miall R C, Weir D J, Wolpert D M and Stein J F 1993 Is the cerebellum a smith predictor? *J. Mot. Behav.* **25** 203–16

Millar S 1997 *Reading by Touch* (New York: Routledge)

Mousty P and Bertelson P 1985 A study of Braille reading: 1. Reading speed as a function of hand usage and context *Q. J. Exp. Psychol.* A **37** 217–33

Mousty P and Bertelson P 1992 Finger movements in braille reading: the effect of local ambiguity *Cognition* **43** 67–84

Newman S E, Hall A D, Foster D J and Gupta V 1984 Learning as a function of haptic discriminability among items *Am. J. Psychol.* **97** 359–72

Nicolelis M A L and Lebedev M A 2009 Principles of neural ensemble physiology underlying the operation of brain–machine interfaces *Nature Rev. Neurosci.* **10** 530–40

Nolan C Y and Kederis C J 1969 *Perceptual Factors in Braille Word Recognition* (New York: American Foundation for the Blind)

Oddo C M, Controzzi M, Beccai L, Cipriani C and Carrozza M C 2011 Roughness encoding for discrimination of surfaces in artificial active-touch *IEEE Trans. Robot.* **27** 522–33

O'Doherty J E, Lebedev M A, Ifft P J, Zhuang K Z, Shokur S, Bleuler H and Nicolelis M A 2011 Active tactile exploration using a brain–machine–brain interface *Nature* **479** 228–31

Passot J-B, Sheynikhovich D, Duvelle E and Arleo A 2012 Contribution of cerebellar sensorimotor adaptation to hippocampal spatial memory *PLoS ONE* **7** e32560

Petrovskaya A and Khatib O 2011 Global localization of objects via touch *IEEE Trans. Robot.* **27** 569–85

Phillips J, Johansson R and Johnson K 1990 Representation of braille characters in human nerve fibres *Exp. Brain Res.* **81** 589–92

Phillips J R, Johansson R S and Johnson K O 1992 Responses of human mechanoreceptive afferents to embossed dot arrays scanned across fingerpad skin *J. Neurosci.* **12** 827–39

Phillips J R, Johnson K O and Hsiao S S 1988 Spatial pattern representation and transformation in monkey somatosensory cortex *Proc. Natl Acad. Sci. USA* **85** 1317–21

Pleger B and Villringer A 2013 The human somatosensory system: from perception to decision making *Prog. Neurobiol.* **103** 76–97

Pruszynski A, Jenmalm P and Johansson R S 2011 Information processing in human tactile afferent neurons *Neuroscience Annu. Meeting* (Washington DC, USA: Society for Neuroscience) abstract no. 750.07

Raspopovic S, Capogrosso M, Badia J, Navarro X and Micera S 2012 Experimental validation of a hybrid computational model for selective stimulation using transverse intrafascicular multichannel electrodes *IEEE Trans. Neural Syst. Rehabil. Eng.* **20** 395–404

Romano J M, Hsiao K, Niemeyer G, Chitta S and Kuchenbecker K J 2011 Human-inspired robotic grasp control with tactile sensing *IEEE Trans. Robot.* **27** 1067–79

Ros E, Carrillo R, Ortigosa E M, Barbour B and Agís R 2006 Event-driven simulation scheme for spiking neural networks using lookup tables to characterize neuronal dynamics *Neural Comput.* **18** 2959–93

Saal H P, Ting J-A and Vijayakumar S 2010 Active estimation of object dynamics parameters with tactile sensors *Proc. IEEE/RSJ Int. Conf. on Intelligent Robots and Systems* pp 916–21

Saal H P, Vijayakumar S and Johansson R S 2009 Information about complex fingertip parameters in individual human tactile afferent neurons *J. Neurosci.* **29** 8022–31

Sánchez E, Barro S, no J Mari and Canedo A 2006 Cortical modulation of dorsal column nuclei: a computational study *J. Comput. Neurosci.* **21** 21–33

Schreiber S, Fellous J M, Whitmer D, Tiesinga P and Sejnowski T J 2003 A new correlation-based measure of spike timing reliability *Neurocomputing* **52–54** 925–31

Shannon E 1948 A mathematical theory of communication *Bell Syst. Tech. J.* **27** 379–423, 623–656

Shimojo M and Ishikawa M 1993 An active touch sensing method using a spatial filtering tactile sensor *Proc IEEE Int. Conf. on Robotics and Automation* vol 1 pp 948–54

Spigler G, Oddo C M and Carrozza M C 2012 Soft-neuromorphic artificial touch for applications in neuro-robotics *Proc. IEEE/RAS/EMBS Int. Conf. on Biomedical Robotics and Biomechatronics* pp 1913–18

Su Z, Fishel J A, Yamamoto T and Loeb G E 2012 Use of tactile feedback to control exploratory movements to characterize object compliance *Front. Neurorobot.* **6**

Thach W T, Goodkin H P and Keating J G 1992 The cerebellum and the adaptive coordination of movement *Annu. Rev. Neurosci.* **15** 403–42

Truccolo W, Friehs G M, Donoghue J P and Hochberg L R 2008 Primary motor cortex tuning to intended movement kinematics in humans with tetraplegia *J. Neurosci.* **28** 1163–78

van Rossum M C 2001 A novel spike distance *Neural Comput.* **13** 751–63

Victor J D and Purpura K P 1996 Nature and precision of temporal coding in visual cortex: a metric-space analysis *J. Neurophysiol.* **76** 1310–26

Whitsel B L, Petrucelli L M and Sapiro G 1969 Modality representation in the lumbar and cervical fasciculus gracilis of squirrel monkeys *Brain Res.* **15** 67–78

Wolpert D M and Miall R C 1996 Forward models for physiological motor control *Neural Netw.* **9** 1265–79

Wolpert D M, Miall R C and Kawato M 1998 Internal models in the cerebellum *Trends Cogn. Sci.* **2** 338–47

Yodogawa E 1982 Symmetropy, an entropy-like measure of visual symmetry *Percept. Psychophys.* **32** 230–40

Yousef H, Boukallel M and Althoefer K 2011 Tactile sensing for dexterous in-hand manipulation in robotics: a review *Sensors Actuators* A **167** 171–87

Zhang H 2004 The optimality of naive Bayes *Proc. FLAIRS Conf.*